Optical, magnetic, and single-particle excitations in the multiband Hubbard model for cuprate superconductors

J. Wagner
Physikalisches Institut, Universität Würzburg, Am Hubland, D-8700 Würzburg, Germany

W. Hanke* and D. J. Scalapino
Department of Physics, University of California, Santa Barbara, California 93106
(Received 23 October 1990)

On the basis of exact diagonalizations, a comparative study of two-particle optical and magnetic, as well as single-particle, excitations is presented for a two-dimensional (2D) multiorbital Hubbard model. For reasonable parameter sets appropriate for the cuprate superconductors, the single-particle excitations display strongly correlated states related to the Zhang-Rice Cu-O singlet construction. These states define the gap (to the upper Hubbard band) at half-filling and become partially occupied by doping holes in our 2×2 unit-cell system. The optical results, which are the first quantitative calculations performed for realistic parameters of the three-band Hubbard model, clearly show three allowed optical transitions: (i) itinerant motion of the Cu-O singlets, having (for doping concentrations $x\neq0$) a spectral Drude distribution around $\omega=0$ with spectral weight proportional to x; (ii) unbinding of the O hole from the Cu spin in the singlet. This gives, in particular, a strong absorption peak due to singlet$\rightarrow$nonbonding oxygen transitions, again with relative weight $\sim x$. It is roughly centered at $\omega\sim J_{\rm Kondo}<\Delta$, where $J_{\rm Kondo}$ is the Kondo coupling and Δ the bare Cu-O charge-transfer energy. It is this singlet unbinding that results in the by far dominant absorption structure between Drude and higher-energy Cu-O transitions and not the often discussed "mid-infrared" absorption due to transitions between different singlet states. (iii) Cu-O charge-transfer processes at energy $\sim\Delta+U_{pd}$. They show a pronounced excitonic effect due to the p-d interaction U_{pd} and have a reduced spectral weight shifted to higher energies for increased dopings. Findings (i)–(iii) are in general accordance with recent experimental data. Our study of the low-energy absorption is complemented with a numerical scaling analysis of the Drude weight in 1D, where, in particular, we find an interesting violation of Lenz's law for $4n$-site Hubbard rings. Finally, the magnetic structure factor is calculated for the 2D case. For finite doping it contains a peak at $2J_{\rm Kondo}$, which should be detectable in experiment.

I. INTRODUCTION

Strongly correlated electronic systems that are close to a metal-insulator transition have been the subject of renewed interest lately. Examples are the heavy-electron systems[1] and most recently the high-temperature cuprate superconductors.[2,3] Close to the transition to the antiferromagnetic insulating state the latter systems display a strongly enhanced effective mass and spin susceptibility.[2] Being simultaneously close to the metal-superconductor transition it is clearly of importance to get a reliable handle on the normal state properties in the vicinity of a Mott-Hubbard type of transition.[4] Our aim in this paper is to derive, for a generalized two-dimensional (2D) Hubbard model, a coherent picture of electronic single-particle (as extracted from direct and inverse photoemission) and two-particle (optical and magnetic) excitations near such a transition.

In Hubbard-type models[4,5] for the high-T_c cuprates, the competition between the kinetic and short-range Coulomb energies gives rise to the possible Mott-Hubbard or charge-transfer–induced metal-insulator transition. In spite of a variety of perturbative, variational, and numerical calculations, the physical consequences that arise from this competition are not yet fully understood.[3] Here we explore the metal-insulator transition, as well as general properties of a multiorbital 2D and, as a preliminary, of a 1D Hubbard model by, in particular, concentrating on the optical excitation spectrum. The corresponding two-particle and also the single-particle Green's functions are calculated using the Lanczos method to exactly diagonalize finite clusters.

The 1D study of the optical conductivity in Sec. II aims mainly at getting the influence of finite-size effects and of varying boundary conditions (open versus periodic) under control. Quite generally, the optical excitations in low-dimensional lattice models have recently enjoyed a renewed interest,[6–15] partly in view of the sensitivity of the low-frequency conductivity, i.e., the Drude spectral weight D to the metal-insulator transition.[9–12,14–16] For the 1D Hubbard model, we find D at half-filling to vanish exponentially with system size N (up to $N=12$) on a length scale set by the inverse gap. However, for finite-sized rings with $N=4n$ sites D is negative ($N=4n+2$, $D>0$), reflecting paramagnetic response and an interesting violation of Lenz's law. Away from half-filling, D tends to a constant diamagnetic value indicating metallic behavior. Recent Bethe-ansatz solutions by Fye, Mar-

tins, Scalapino, Wagner, and Hanke[15] up to $N=64$ sites further corroborate these results.

In Sec. III the single-particle and two-particle (optical and magnetic) excitations are calculated for the Emery model,[5] which, as a three-orbital Hubbard model, explicitly takes into account that holes introduced by doping go preferentially on O sites. One central result of our study in Sec. III is that the Zhang-Rice type of singlet construction[17] plays not only a crucial role for the "low-energy" physics as in the t-J model, but is of significance also for the "higher-energy" physics (up to several eV) as probed in an optical absorption experiment. Zhang and Rice proposed that the three-band Hubbard model can be simplified in the relevant parameter regime via a singlet formation between the Cu hole and the doped O hole to the t-J model.[17] The energy scales left in this model are merely of lower energy, i.e., $J\sim 0.1$ eV and $t\sim 1$ eV.

Specifically, we find the single-particle excitations for the three-band Hubbard model at half-filling to display strongly correlated states. These states are of singlet character, are located at the top of the valence "bands," and form the charge-transfer gap to the upper Hubbard band. This renormalized charge-transfer gap can be obtained in agreement with experimental values both by choosing a relatively large value of the on-site transfer energy Δ, or, alternatively, a smaller value of Δ, however, with a finite p-d Coulomb repulsion U_{pd}. Similar diagonalization results for the single-particle spectrum of the Emery model have recently been obtained by Horsch *et al.*[18]

When we try to reconcile single-particle and, additionally, two-particle optical spectra at half-filling with experiment, we are led to the interesting conclusion that a finite U_{pd} of the order of t_{pd} (p-d hopping), together with a value of $\Delta\simeq 2t_{pd}$, is required. This is related to the fact that the dominant Cu-O charge-transfer transition is found to be shifted to lower energies by an excitonic energy of order U_{pd}. To study the finite-size effect, system sizes up to $N=18$ have been diagonalized at half-filling.

Doping one or two holes in our 2×2 unit cell (12-site) system introduces the insulator-metal transition and moves the Fermi level into the band complex of highly correlated states. Therefore, these singlet states become a reservoir for possible optical transitions. Three related absorption structures can clearly be identified.

(a) First, the Drude peak with its spectral distribution around $\omega=0$, and, in agreement with experiment,[19] its weight proportional to the doping concentration x.

(b) Second, a small structure due to transitions within the singlet band complex, which may be related to the experimentally observed midinfrared absorption.[3,19] Both transitions (a) and (b) stem from itinerant motion of the Zhang-Rice–type singlets.

(c)Third, a previously undetected strong absorption structure which corresponds to the unbinding of the O hole from the Cu spin in the singlet. It is centered roughly at the Kondo-coupling energy $\omega\sim J_{\rm Kondo}<\Delta$, and has again a relative weight $\sim x$. We believe that this structure (at least for $x\gtrsim 0.2$) is very likely the dominant contribution to the optical spectral weight found in experimental data[3,19] between Drude and higher-energy charge-transfer peaks. In general accord with experiment is also the reduction and shift to even somewhat higher energies of the latter charge-transfer–related spectral weight, when the system is doped.

Finally, our calculation of the dynamic magnetic-structure factor reveals a strong absorption at the Kondo-like spin(Cu)-spin(O) correlation energy $2J_{\rm Kondo}$, when the system is doped away from half-filling. This signal, which is related to the singlet-triplet excitation energy of the doping-induced Zhang-Rice Cu-O spin-hole singlet state, should be observable at an energy of the order $2J_{\rm Kondo}\sim t_{pd}\sim 1.5$ eV in magnetic absorption experiments.

II. OPTICAL ABSORPTION FOR HUBBARD MODELS: SUMMARY OF LINEAR-RESPONSE THEORY AND 1D RESULTS

In Sec. II A the results of linear-response theory, which are needed in the following discourse, are summarized. In particular, the Drude spectral weight D is introduced, which, as a direct measure of a possible metal-insulator transition, has recently been a focus on renewed attention.[9–11,15] Section II B gives a short summary of the Lanczos method, and Sec. II C presents our exact diagonalization results for the 1D Hubbard model.

A. Optical conductivity and Drude spectral weight

Since we are primarily interested in applying the formalism to the high-T_c compounds, we start from a generalized Hubbard model with the Hamiltonian

$$H=\sum_{\substack{i,j,\\ \sigma}}\varepsilon_{ij}c_{i\sigma}^{\dagger}c_{j\sigma}+\tfrac{1}{2}\sum_{\substack{i,j\\ \sigma,\sigma'}}U_{ij}n_{i\sigma}n_{j\sigma'}\ . \tag{2.1}$$

If the model (2.1) is specialized to the CuO_2 2D layers, $c_{i\sigma}^{\dagger}$ creates a hole with spin σ in the Cu $d_{x^2-y^2}$ or the O $p_{x,y}$ orbital with occupation number operator $n_{i\sigma}$, depending on the lattice site i. ε_{ij} contains the on-site energies ε_d(Cu) and ε_p(O) with the charge-transfer energy $\Delta=\varepsilon_p-\varepsilon_d$, and nearest-neighbor hoppings t_{pd} (including the usual d- and p-orbital phase factor) and t_{pp}. The interaction part is due to the on-site repulsions U_d and U_p, and a nearest-neighbor Cu-O repulsion U_{pd}. The units used in the following are $\hbar=c=1=e$, and also $a=1$ for the lattice constant.

The optical conductivity represents the real part of the linear response of the lattice fermionic system in Eq. (2.1) to a uniform time-dependent electric field in, say, y direction. This electric field may be generated by threading the system with a flux $\Phi(t)$,[16] which is represented by a vector potential $\mathbf{A}(t)=[\Phi(t)/N_y]\hat{y}\equiv(0,A)$, where N_y is the number of sites in y direction (total number of sites is equal to N). As a consequence the nearest-neighbor (NN) hopping term t_{pd} in Eq. (2.1) acquires a constant phase $\exp[\pm iA(y_i-y_j)]$, where y_i and y_j denote NN (Cu and O) positions along the y direction.

Expanding H in Eq. (2.1) to second order in A, one obtains the perturbed Hamiltonian[6]

$$H(A)=H-A(t)j_p-\frac{\tau^2}{2}A^2(t)T_y+O(A^3)\ , \tag{2.2}$$

where T_y is the kinetic energy in the direction of the applied field, i.e.,

$$T_y=\sum_{i,\sigma}t_{pd}(c^\dagger_{i\sigma}c_{i+\hat{y}\tau,\sigma}+c^\dagger_{i\sigma}c_{i-\hat{y}\tau,\sigma}), \tag{2.3}$$

with $\pm\hat{y}\tau$ denoting the NN sites of site i along $\hat{y}$. τ is the distance between two NN sites in units of the lattice constant a (e.g., $\tau=\frac{1}{2}$ for the 2D CuO_2 layers; $\tau=1$ for the 1D Hubbard model). j_p denotes the "paramagnetic" current operator in the y direction:

$$j_p=i\tau\sum_{i\sigma}t_{pd}(c^\dagger_{i\sigma}c_{i+\hat{y}\tau,\sigma}-c^\dagger_{i\sigma}c_{i-\hat{y}\tau,\sigma})\ . \tag{2.4}$$

The total physical current $\langle -[dH(A)/dA]\rangle$ contains the paramagnetic plus diamagnetic contributions.[16]

In linear response, the usual formula for the complex conductivity results:

$$\sigma(\omega)=\frac{1}{i\omega}\left[\frac{\tau^2}{N}\langle 0|T_y|0\rangle-\chi(\omega)\right]\ , \tag{2.5}$$

with the current-current correlation function [$|n\rangle=|\Phi_n(A=0)\rangle$]

$$\chi(\omega)=\frac{1}{N}\sum_n|\langle 0|j_p|n\rangle|^2\left[\frac{1}{\omega-(E_n-E_0)+i\eta}-\frac{1}{\omega+(E_n-E_0)+i\eta}\right]\ . \tag{2.6}$$

Decomposing Eq. (2.5) into real (σ') and imaginary (σ'') parts, one arrives at

$$\sigma'(\omega)=D\delta(\omega)+\sigma'_{\rm reg}(\omega) \tag{2.7}$$

and

$$\sigma''(\omega)=\frac{1}{\omega}\left[\frac{\tau^2}{N}\langle 0|-T_y|0\rangle+{\rm Re}\chi(\omega)\right]\ . \tag{2.8}$$

The second term in Eq. (2.7), i.e., $\sigma'_{\rm reg}(\omega)=-(1/\omega){\rm Im}\chi(\omega)$, is generally present both in metallic and insulating systems and arises from $n\neq 0$ transitions only [$\sigma'_{\rm reg}(\omega=0)=0$]. The remaining nonregular part is defined by the Drude spectral weight:

$$D=\frac{\pi\tau^2}{N}\langle 0|-T_y|0\rangle+\pi\,{\rm Re}\chi(\omega\to 0)\ . \tag{2.9}$$

As discussed originally by Kohn[16] and more recently by Shastry and Sutherland,[9] Millis and Coppersmith,[11] Schulz,[10] and Fye *et al.*,[15] D serves as a direct and sensitive measure of a metal-insulator transition. On the basis of Lanczos diagonalization of the 1D Hubbard model this will be further corroborated in Sec. II C.

The Drude weight D, which is inversely proportional to the effective optical mass, can also be extracted from the energy shift in the ground state in the presence of the field, i.e.,[16]

$$\frac{1}{N}\frac{d^2E_0(A)}{dA^2}\bigg|_{A=0}=\frac{D}{\pi}=\lim_{\omega\to 0}\omega\sigma''(\omega)\ . \tag{2.10}$$

Another useful relation, which is needed in the following discourse, is the well-known f-sum rule[6,7]

$$\int_0^\infty\sigma'(\omega)d\omega=\frac{\pi\tau^2}{2N}\langle 0|-T_y|0\rangle\ , \tag{2.11}$$

which immediately derives from putting Eq. (2.7) with (2.9) into (2.11) for $\sigma'(\omega)$ or, equivalently, by making use of the high-frequency result

$$\lim_{\omega\to\infty}\omega\sigma''(\omega)=\frac{\tau^2}{N}\langle 0|-T_y|0\rangle\ ,$$

from Eq. (2.8).

Up to now we have not specified the boundary conditions. Consider first open boundary conditions (OBC) in the direction of the electric current and periodic boundary conditions (PBC) perpendicular to it. The length of the system in the y (current) direction is L. Then

$$\int_0^\infty\sigma'(\omega)d\omega=\int_0^\infty\sigma'_{\rm reg}(\omega)=\frac{\pi}{N}\sum_{n\neq 0}\frac{|\langle 0|j_p|n\rangle|^2}{E_n-E_0}, \tag{2.12}$$

since, in this case, the Drude or free acceleration part in Eq. (2.7) vanishes. Equation (2.12) just shows that, in a metallic system with finite length L, we cannot observe free acceleration and optical absorption at $\omega=0$, contrary to infinite systems. This finite-size effect limits the lowest-energy scale due to the limit on the largest-length scale. Thus, for finite metallic systems we expect a "Drude precursor" (see Sec. II C) around this minimum excitation energy ω_D. In other words, for OBC the Drude weight D can be extracted from finite-size scaling of the right-hand-side expression of Eq. (2.12) (see again the explicit verification in Sec. II C).

As has already been shown by Maldague[6] the sum rule, Eq. (2.11), is fulfilled in this OBC case, and $\sigma'_{\rm reg}(\omega)=-(1/\omega){\rm Im}\chi(\omega)$ in Eq. (2.12) exploits all optical transitions in systems with confined length L.

In contrast, for periodic boundary conditions (PBC) in current direction, the particles can freely accelerate; the coefficient D [calculated from Eq. (2.9) or (2.10)] of $\delta(\omega)$ in $\sigma'(\omega)$ is nonzero, implying an infinite dc conductivity.

B. Lanczos diagonalization

Since throughout this article numerical results are obtained from exact diagonalization of finite clusters, let us briefly indicate the diagonalization procedure.[20] The method used to calculate the optical, magnetic, and single-particle spectral functions is a generalization of the recursion method of Haydock, Heine, and Kelly[21] based on the Lanczos algorithm.[22]

Typically, we have an expression as in Eq. (2.7) for the real part of the conductivity; i.e.,

$$\sigma'_{\rm reg}(\omega)=-\frac{1}{\omega}{\rm Im}\chi(\omega+i\eta)\ , \tag{2.13}$$

where

$$\chi(z)=\frac{1}{N}\langle 0|j_p(z+E_0-H)^{-1}j_p|0\rangle \ . \tag{2.14}$$

Starting with a trial wave function $|\Phi_0\rangle$, a sequence of orthogonal functions $|\Phi_n\rangle$ is generated by the recursion relation

$$|\Phi_{n+1}\rangle=(H-a_n)|\Phi_n\rangle-b_n^2|\Phi_{n-1}\rangle \ , \tag{2.15}$$

where $a_n=\langle\Phi_n|H|\Phi_n\rangle/\langle\Phi_n|\Phi_n\rangle$, $b_n^2=\langle\Phi_n|\Phi_n\rangle/\langle\Phi_{n-1}|\Phi_{n-1}\rangle$, and $b_0=0$. Usually less than 100 Lanczos steps are required in order to achieve good convergence for the ground-state wave function $|0\rangle$ and energy E_0. $|0\rangle$ is obtained by the diagonalization of a tridiagonal matrix with elements a_n and b_n. In order to evaluate the current-current response function χ in Eq. (2.13) or, similarly, the spin-spin response in Sec. III C, we run through the same Lanczos procedure as in Eq. (2.15), but with an initial wave function $|\tilde{\Phi}_0\rangle\equiv j_p|0\rangle$.

In the general case $|\tilde{\Phi}_0\rangle\equiv A|0\rangle$, where $A\equiv\sum_i S_i^z\exp(i\mathbf{q}\cdot\mathbf{R}_i)$ for the spin response (Sec. III C), or $A\equiv c_{i\sigma}$, if we consider the one-particle Green's function (Sec. III A). Then $\chi(z)$ can be expressed with Lanczos corresponding coefficients α_n,β_n in the form of continued fractions

$$\chi(z)=\frac{1}{N}\cfrac{\langle 0|A^\dagger A|0\rangle}{z-\alpha_0-\cfrac{\beta_1^2}{z-\alpha_1-\cfrac{\beta_2^2}{z-\cdots}}} \ . \tag{2.16}$$

In a finite system $\chi(z)$ has poles on the real axis. The convergence for the essential optical features emerging from Eq. (2.16) can typically be achieved after about 100 Lanczos steps.

C. Scaling of the Drude spectral weight and optical absorption for the 1D Hubbard model

In order to illustrate some of the discussions in Sec. II A and to prepare the ground for a careful study of the low-frequency conductivity of the 2D Hubbard model, we study here the size dependence of the Drude weight D. D is extracted from exact diagonalizations as a function of N for different values of U/t and band filling $\langle n\rangle=\langle n_{i\uparrow}+n_{i\downarrow}\rangle$ of the N-site one-dimensional, single-band Hubbard model [$t_{pd}\equiv t$, $U_{pd}=0=U_p$ in Eq. (2.1)] with

$$H=-t\sum_{i,\sigma}(c_{i,\sigma}^\dagger c_{i+1,\sigma}+\text{H.c.})+U\sum_i n_{i\uparrow}n_{i\downarrow} \ . \tag{2.17}$$

Before going into details of our calculation, let us comment on recent literature, which aims at using the Drude weight as a probe of a possible metal-insulator transition. Shastry and Sutherland[9] have studied the 1D Heisenberg-Ising model and calculated the optical effective mass by using the Bethe ansatz. They also point out some general relations for the 1D Hubbard model. Millis and Coppersmith[11] have interpreted the Drude weight D and the f-sum rule weight in (2.11) as "coherent" and "incoherent" plasma frequencies and derived some general results employing variational wave functions for the 2D Hubbard model. A similar exact diagonalization study was carried out for 1D t-J clusters by Zotos, Prelovšek, and Sega[12] and for 2D t-J clusters by Poilblanc and Dagotto.[14] Schulz[10] has evaluated the ratio of the Drude weight to the total (f-sum rule) spectral weight for the infinite 1D Hubbard chain.

However, none of these calculations has focused on the scaling dependence of these quantities with N for various values of U/t and filling $\langle n\rangle=\langle n_{i\uparrow}+n_{i\downarrow}\rangle$. Following the general arguments of Kohn,[16] it is precisely this scaling of the zero-frequency optical spectral weight with the linear dimension of the system which can be used as a probe of the metal-insulator transition.

We start with the size dependence of D versus N with $U/t=12$ for PBC rings up to 12 sites in Fig. 1. These results are obtained from Eq. (2.9). For $N=4n$ rings, D is negative, indicating that the diamagnetic ($-\langle 0|T|0\rangle$) contribution in (2.9) is smaller than the paramagnetic Van Vleck term. At half-filling D vanishes like $D\sim\exp(-N/\xi)$, where the localization length ξ of the carriers depends on U/t. This is depicted in Fig. 2.

One may also extract from Figs. 1 and 2 and the Lanczos results that the localization length ξ varies as t/Δ, where Δ is the gap for the half-filled ring (see, in particular, the recent numerical scaling results obtained from Bethe-ansatz solutions up to $N=64$ by Fye *et al.*[15]).

The physical reason for the sign change has been clarified in Ref. 15. Summarizing the argument, consider the four-site ring with four electrons in the small (U/t) limit and its energy diagram in Fig. 3. The leading-order dipole transition is given by the bonding-antibonding transition

$$\tfrac{1}{2}\langle\psi_{\text{III}}-\psi_{\text{IV}}|j_p|\psi_{\text{III}}+\psi_{\text{IV}}\rangle=4t \ ,$$

and the kinetic energy expectation value by

$$\tfrac{1}{2}\langle\psi_{\text{III}}-\psi_{\text{IV}}|T|\psi_{\text{III}}-\psi_{\text{IV}}\rangle=-4t \ ,$$

so that for small values of U/t

$$D=\pi t\left[1-\frac{16t}{U}\right] \ . \tag{2.18}$$

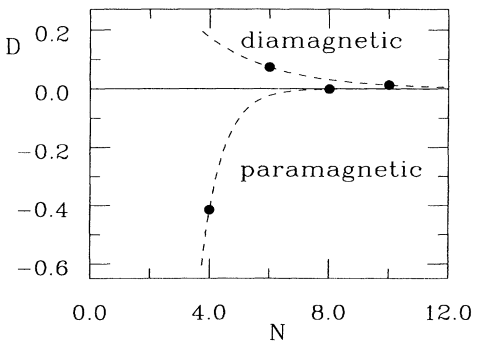

FIG. 1. D vs N for $U/t=12$ and $\langle n\rangle=1$. Half-filled rings with $N=4n+2$ sites are diamagnetic ($D>0$); rings with $N=4n$ are paramagnetic ($D<0$).

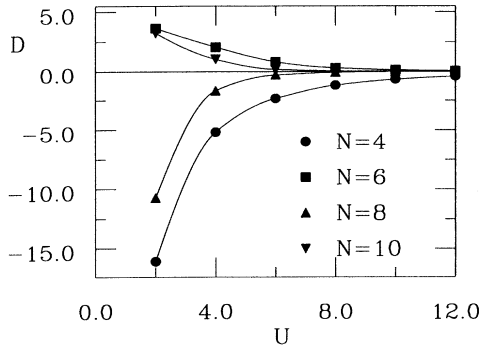

FIG. 2. D (PBC) plotted vs U for $\langle n \rangle = 1$ and various lengths N.

Thus, the Drude weight is negative and diverges to $-\infty$ as $U \to 0$.

Alternatively viewed, since the expansion of the ground-state energy $E_0(A)$ in the presence of the vector potential A, as in Eq. (2.2), is

$$E_0(A) = E_0(0) - A\langle j_p \rangle + \frac{N}{2} A^2 \frac{D}{\pi} + O(A^4) , \qquad (2.19)$$

a negative Drude weight lowers the ground-state energy for a finite value of A ($\langle j_p \rangle$ vanishes in the half-filled ring). This can also be immediately seen from the ε_k diagrams for states (III) and (IV) in Fig. 3: It is clear that the ground state acquires a lower minimum than the $A = 0$ case by shifting the momentum k in (III) and (IV) by $k \pm \pi/N$, where $\Phi_\pm = \pm\pi/N$ directly corresponds to the applied vector potential A. This behavior is also confirmed by direct calculation of $E_0(A)$.[15] As already noted in Ref. 15 this interesting result for the n-site rings does not have as a consequence an instability with respect to spontaneous current flow and flux generation.[15] The above result implies, however, a violation of the familiar Lenz law: If D is negative, the induced currents produced by an external B-field flow in the opposite direction of the diamagnetic loop currents, as constructed by Lenz's law. The microscopic reason for this astonishing result is indicated in Fig. 3: For $N = 4n$-site rings umklapp processes provide a coherent mixing of states (III) and (IV), with pairs of electrons in these states circulating in opposite directions.

In contrast to this, for half-filled rings with $N = 4n + 2$ sites, we have a "closed-shell" situation. Following the same steps as those leading to Fig. 3, one immediately sees that here $E_0(A)$ acquires a minimum at $A = 0$, and thus $D > 0$.

When we depart from half-filling, D remains positive as the number of lattice sites N increases. In this case, the Hubbard ring is metallic, with the ratio $(n/m)^* > 0$. Figure 4 displays D versus the number of charge carriers $x = |1 - \langle n \rangle|$ for rings with PBC. How are these results affected, if one changes from the periodic to the open boundary conditions (OBC)?

Figure 4 contains additional results for $U/t = 12$ for open chains with 10 sites. These results were obtained by integrating over the Drude precursor, i.e.,

$$\begin{aligned} \int_{\text{precursor}} \sigma'(\omega) d\omega &\equiv \int_0^\infty \sigma'(\omega) d\omega - \int_{\neq \text{precursor}} \sigma'(\omega) d\omega \\ &= \frac{\pi \tau^2}{2N} \langle 0 | -T_y | 0 \rangle - \int_{\neq \text{precursor}} \sigma'(\omega) d\omega \\ &= \frac{D}{2} . \end{aligned} \qquad (2.20)$$

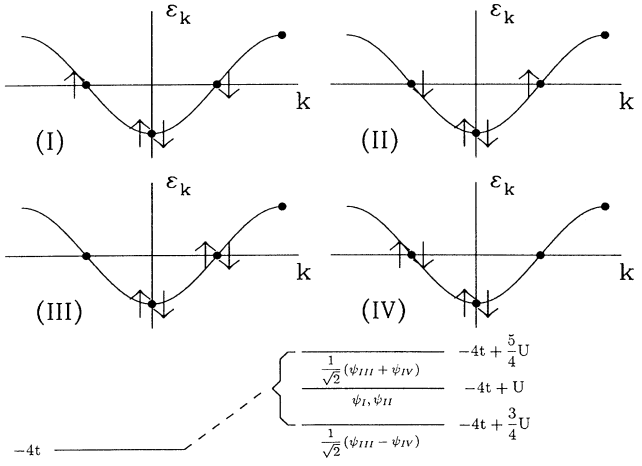

FIG. 3. Schematic energy-level structure for the half-filled $N = 4$ ring. For $U = 0$, the four states (I–IV) are degenerate with energy $-4t$. In the presence of U this degeneracy is lifted and the new nondegenerate ground state $(\psi_{III} - \psi_{IV})/\sqrt{2}$ splits off.

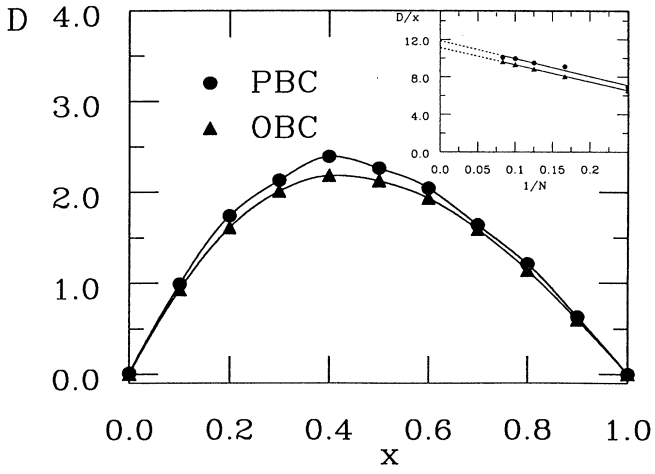

FIG. 4. Drude weight D vs x in the strong-coupling case $U/t = 12$ for rings [PBC, Eq. (2.9)] and chains [OBC, Eq. (2.20)]. The system consists of $N = 10$ sites. In the inset the system size is varied from $N = 4$ up to $N = 12$ to extrapolate the relative Drude weight D/x near half filling to the thermodynamic limit.

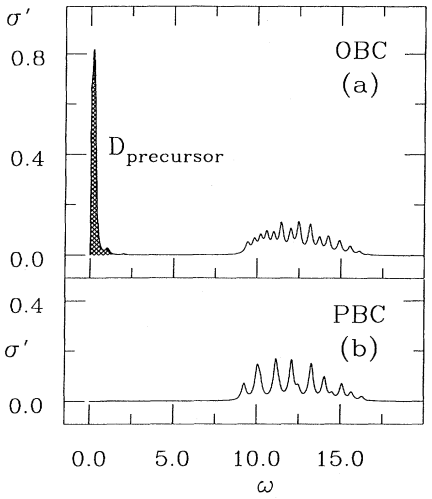

FIG. 5. Optical absorption for $U/t=12$, one-hole doped, $N=12$: (a) open boundary conditions with the Drude precursor; (b) periodic boundaries. A broadening $\eta=0.15$ has been used to smooth out $\sigma'(\omega)$.

It is obvious that the PBC [Eq. (2.9)] and the OBC [Eq. (2.20)] methods yield, within numerical accuracy, identical results for D versus x. For low doping we find the Drude weight proportional to the number of charge carriers x. This has recently also been pointed out near half-filling by Schulz[10] and confirmed by Bethe-ansatz solutions.[15] In the inset of Fig. 4 finite-size extrapolations to the thermodynamic limit are done by plotting D/x versus $1/N$ for the one-hole doped situation ($x=1/N$). Thus, we obtain $D=(11.5\pm0.3)x$ near half-filling for $U/t=12$ in the thermodynamic limit. Figure 5 gives the optical absorption for a given parameter set ($U/t=12$, $x=1/12$, $N=12$) for both boundary conditions and indicates the evaluation of the Drude weight as it enters Fig. 4.

Finally, in Fig. 6 the total spectral weight $-\langle 0|T|0\rangle/N$ is plotted versus x for different values of U/t. As $x\to 0$ or $\langle n\rangle$ approaches half-filling ($\langle n\rangle=1$), D vanishes, but the total spectral weight remains finite. In this way the optical conductivity and, in particular, the "stiffness"[9] D serves as an order parameter for the metal-insulator transition, i.e., the Mott-Hubbard transition. Of course, this also remains true for the 2D multiband Hubbard model studied in the following section, where the gap can also be induced by a charge-transfer mechanism.

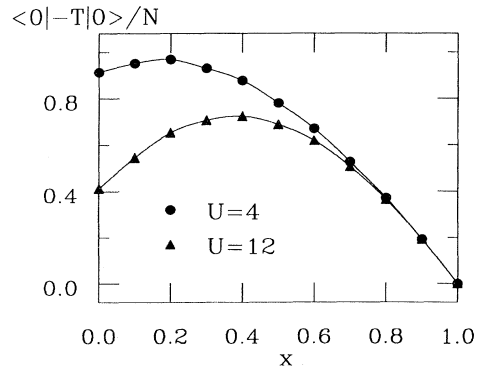

FIG. 6. Total strength weight $-\langle 0|T|0\rangle/N$ as a function of filling $x=|1-\langle n\rangle|$. The curves connecting calculational results are guides to the eye.

III. SINGLE-PARTICLE AND TWO-PARTICLE (OPTICAL, MAGNETIC) EXCITATIONS FOR THE 2D MULTIBAND HUBBARD MODEL

A. Single-particle excitations

The spectral weight for single-particle excitations may be defined as

$$g_{i\sigma}(\omega)=g_{i\sigma}^{>}(\omega)+g_{i\sigma}^{<}(-\omega)\ , \tag{3.1}$$

where

$$g_{i\sigma}^{>}(\omega)=\sum_n |\langle \psi_n(N+1)|c_{i\sigma}^{\dagger}|\psi_0(N)\rangle|^2 \times\delta(\omega-E_0(N)+E_n(N+1))\ , \tag{3.2}$$

with $c_{i\sigma}$ replacing $c_{i\sigma}^{\dagger}$ and $N-1$ replacing $N+1$ in the expression for $g_{i\sigma}^{<}(\omega)$. $|\psi_0(N)\rangle$ is the N-hole ground state, and $|\psi_n(N+1)\rangle$ an eigenstate of the $(N+1)$-hole system, having energies $E_0(N)$ and $E_n(N+1)$, respectively. The single-hole excitations in Eq. (3.2) correspond (ideally) to the photoemission spectra of experiment. On the other hand, $g_{i\sigma}^{<}$ describes the inverse photoemission, where an electron is added to the system.

To implement the Lanczos diagonalization as discussed in the previous section, we note that, for example, the spectral function for adding a hole (photoemission) may be written as

$$g_{i\sigma}^{>}=\frac{1}{\pi}\mathrm{Im}\langle\Phi_0(N+1)|(E+H-i\eta)^{-1}|\Phi_0(N+1)\rangle\ , \tag{3.3}$$

where $|\Phi_0(N+1)\rangle\equiv c_{i\sigma}^{\dagger}|\psi_0(N)\rangle$. Here $E\equiv\omega-E_0(N)$ is the excitation energy measured from the ground-state energy of the N-hole system, and $\eta\to 0^+$. The expression in Eq. (3.3) is evaluated as described in Sec. II B by employing the Lanczos method in two steps: In the first step $|\psi_n(N)\rangle$ is extracted iteratively, as in Eq. (2.15). In the second step, a hole is created in this state. In the case of more than one site per unit cell, as in the CuO_2 model of Eq. (2.1), the creation depends in general on the experimental situation[3]: For example, the creation on Cu or O sites, respectively, can be experimentally monitored by varying the incoming energy. At the incident energies used in the CuO_2 experiments the emission of an electron from a Cu $3d$ state has usually a much larger cross section than the emission from an O $2p$ state.[23] The new state Φ_0 is then again calculated via Lanczos, arriving at

the continued fraction expansion of $(z+H)^{-1}$ in Eq. (2.16). Equivalently, $g^{>}$ may be extracted from the eigenvalues and eigenvectors of the tridiagonal matrix , as in Eq. (2.15). Again a finite value of $\eta=0.2$ leads to a useful smoothing of the spectra, which would otherwise consist of a set of spikes caused by the relatively small number of unit cells (if not stated otherwise—see, however, the optical calculation below—we use $2\times2\equiv4$ CuO_2 unit cells).

The actual electronic structure of high-T_c materials with many particles per unit cell is rather formidable. However, a great deal of simplification arises from the fact that the essential hoppings and Coulomb correlations take place in the 2D CuO_2 plane.[24,25] A further simplification arises because in the undoped (for example, La_2CuO_4) parent compound only one electron (half-filled) per CuO_2 unit cell is missing to fill all bands. The largest hopping integral t_{pd} is between $Cu(d_{x^2-y^2})$ and $O(p_x,p_y)$ orbitals. These orbitals have an energy separation $\Delta\equiv\varepsilon_p-\varepsilon_d$, which, when positive, implies holes going predominantly onto O sites.[5,26,27] This is schematically shown in Fig. 7. Of special importance, because of the antiferromagnetic and insulating nature of the undoped half-filled ground state, is the Hubbard interaction U_d on Cu sites.[4] Additionally, connected with charge transfers, the nearest-neighbor Coulomb repulsion U_{pd} may also become important. Finally, the double occupancy on O sites costs an energy U_p.

If we are in the generally accepted[24,25] charge-transfer regime for the high-T_c compounds, U_d should be larger than Δ. The relatively small energy separation Δ leads to a strong covalent splitting of the p-d-band complex into a bonding and an antibonding band, which is half-filled. Additionally, we have a nonbonding, dispersionless band (if $t_{pp}=0$). If the Coulomb correlation on Cu is turned on, one expects for larger U_d that the metallic antibonding band is split into an upper [(UHB) in the figures] and lower Hubbard band (LHB). These bands correspond to Cu transitions $d^9\rightarrow d^{10}$ and $d^9\rightarrow d^8$, respectively, with the d^{10} final state being shifted by about U_d, as in Fig. 7.

Having prepared the ground for a more detailed discussion of our single-particle spectra, we concentrate in Figs. 8 and 9 on two typical parameter sets: Both sets guarantee insulating behavior due to a charge-transfer gap in the undoped half-filled case. In the first parameter set this is achieved by a relatively large $\Delta=4$ (everywhere in the following energies are measured in units of t_{pd}, where t_{pd} varies according to recent constrained local-density–functional estimates[24,25] between 1.3 and 1.5 eV). In the second set we choose $\Delta=2$, but, additionally, $U_{pd}=1$, which generates in the local energy diagram of Fig. 7 the same charge-transfer gap $\Delta+2U_{pd}$. In both sets, we have chosen $U_d=6$ and $U_p=3$, values which are in good agreement with density-functional estimates.[24,25] Including the intrinsic O bandwidth t_{pp} only introduces small quantitative changes of our results. The underlying physical picture, however, is not modified because of t_{pp} for the proposed[24,25] value $t_{pp}\lesssim\frac{1}{2}t_{pd}$.

Figure 8(a) displays the photoemission and inverse photoemission results as a function of energy for the first parameter set ($\Delta=4$, $U_{pd}=0$) in the undoped case. These calculations are done by using periodic boundary conditions. Because we obtain qualitatively the same results with open boundary conditions, we expect no strong finite-size effects. Solid lines denote the Cu density of

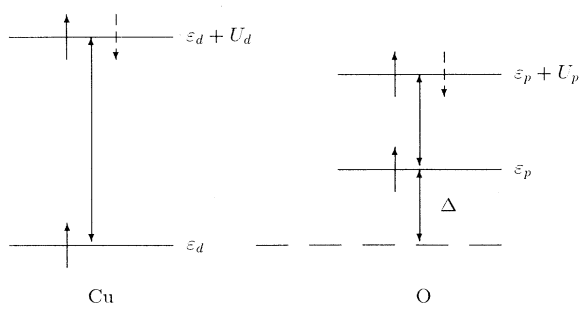

FIG. 7. Local energy diagram (schematically) for the three-band Hubbard model in hole notation.

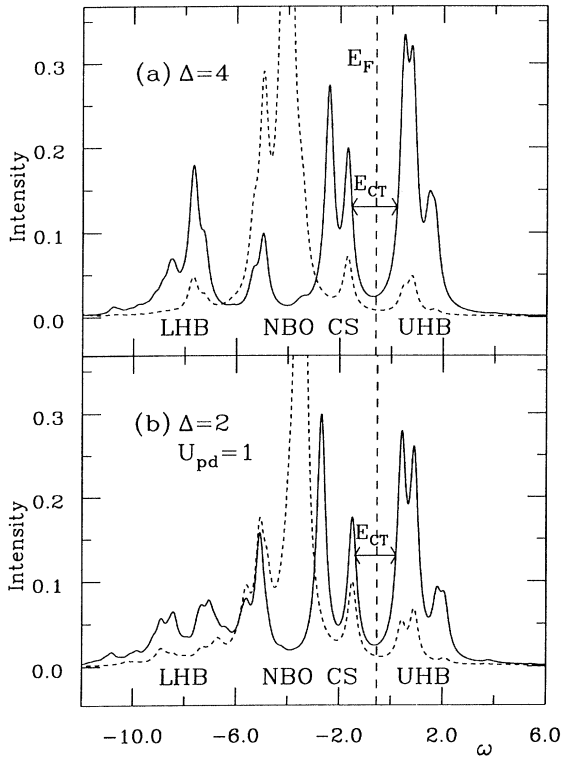

FIG. 8. Photoemission spectra in the undoped system using periodic boundary conditions: (a) $\Delta=4$, $U_d=6$, $U_p=3$; (b) $\Delta=2$, $U_{pd}=1$, $U_d=6$, $U_p=3$. The solid line stands for the creation ($\omega>E_F$) and the annihilation ($\omega<E_F$) of an electron on the Cu site (Cu DOS), whereas the dashed line denotes the O DOS.

states (DOS) and the dashed line stands for the O DOS, where we have averaged over the two O positions in Eqs. (3.1) and (3.2). For example, the O spectrum is related to an O 1s absorption spectrum.[26] Figure 8(b) gives the spectra for $\Delta=2$ and $U_{pd}=1$. Both parameter sets result in nearly identical charge-transfer gaps (E_{CT} in Fig. 8) of about 1.5. This value is in good accord with experiment[3,19] and, interestingly, is also in agreement with recent quantum Monte Carlo results employing the same parameter sets.[28,29] The spectrum of, in particular, the first set with $\Delta=4$ and vanishing U_{pd} distinctively displays the features we have qualitatively discussed above. Due to the relatively large $U_d=6$ the lower (LHB) and upper (UHB) Hubbard bands, which both have small oxygen characters, are well separated by U_d plus a typical hybridization energy. For the parameter sets used in Fig. 8 the LHB for the destruction (photoemission) of an electron on a Cu site (solid line) is in fact due to several peaks originating from a more complex structure. This structure is created by mixing in other final states, e.g., d^9p^5; this is because the ground state fluctuates between d^9p^6 and $d^{10}p^5$. The nonbonding O band (NBO) is the dominant feature in the O spectra. Because the hole density is rather low on O sites in the undoped case, U_p is found to play essentially no role. Finally, an important structure [the correlated states (CS) in Fig. 8] emerges near the Fermi energy (E_F), which has no analog in the band structure. This structure corresponds to highly correlated states. Their physical content has been extracted carefully by examining different two-particle (local singlet- and triplet-) correlation functions. They correspond to the singlet proposed by Zhang and Rice for the doped situation.[17]

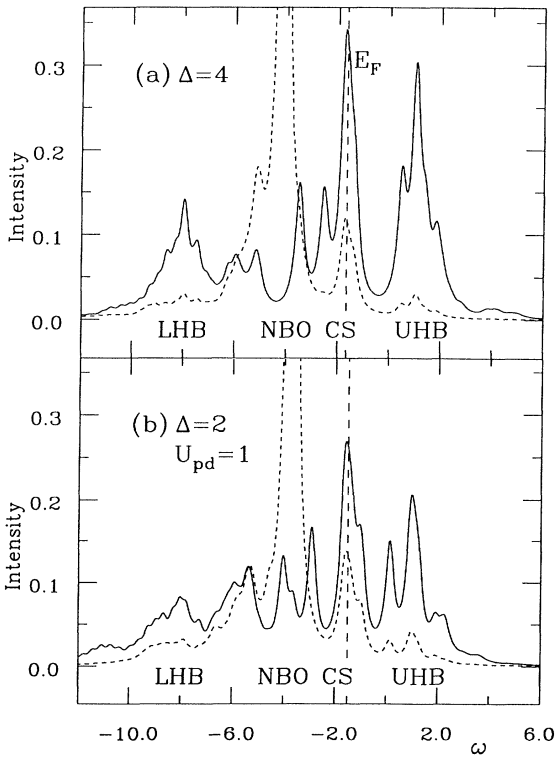

FIG. 9. Same as Fig. 8, but now for the doped system

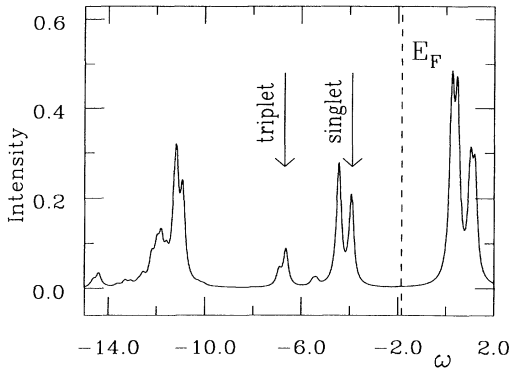

FIG. 10. Cu DOS for $\Delta=6$, $U_d=10$. The two arrows denote the strong-coupling result for the singlet and the triplet state as constructed by Zhang and Rice.

In order to make possible contact with the Zhang-Rice singlet idea, we chose for a moment a different parameter set $U_d=10$, $\Delta=6$. The approximate mapping of the multiband 2D Hubbard model onto an effective single-orbital t-J model becomes exact in the limit of both large Δ and U_d, keeping $U_d-\Delta$ finite.[30] Because of the symmetric combination of oxygen orbitals around a Cu site in the local Zhang-Rice construction[17] the singlet-triplet splitting is given by $8J_{\text{Kondo}}$ in lowest order. Here, J_{Kondo} denotes the strong-coupling value[27,31–33]

$$J_{\text{Kondo}}=t_{pd}^2\left[\frac{1}{\Delta}+\frac{1}{U_d-\Delta}\right]. \tag{3.4}$$

The numerical result for $U_d=10$, $\Delta=6$ in Fig. 10 agrees quite well with the strong coupling result, as denoted by the two arrows representing the singlet and the triplet states, respectively. Thus the feature (CS), which has also been detected in recent Lanczos simulations of the three-band model by Horsch,[34] can be interpreted as a Zhang-Rice–like singlet state.

Figures 9(a) and 9(b) give the corresponding results for the parameter set (a) and (b), when the system is doped with one hole. Still, all the essential features of the undoped case are present, with the most notable change being the shift of the Fermi energy from a position in the charge-transfer gap into the correlated states (CS). We do not observe the dominant feature reported in other work[34] within the energy region corresponding to the gap at half-filling. Because of the finite spectral weight at E_F, we expect metallic behavior, which will be investigated in the following by studying two-particle, i.e., optical and magnetic excitations.

B. Optical excitations

Armed with the knowledge of the single-particle spectra, we can now also extract from the Lanczos method the optical absorption or $\sigma'(\omega)$.

The different geometries used for OBC and PBC are schematically depicted in Fig. 11. For the undoped case, we were also able to study a system with 18 sites (6 sites in the direction of the current j_p).

We start with OBC. Clearly, for the rather small system sizes considered here, the small number of $\mathbf{k}$ points [$\mathbf{k}=(0,0)$, $(\pi,0)$, $(0,\pi)$, (π,π) for 2×2 unit cells] severely limits the optical transitions. Nevertheless, we expect that above the minimum-energy scale ω_D, set by the maximum-length scale N_y, the optical absorption should at least be qualitatively correct.

In the parameter regime, appropriate for the high-T_c superconductors, the one hole per unit cell is mainly localized on the Cu site in the undoped case. Application of the current operator onto this state implies a charge transfer of this hole from the Cu to the O site. Thus, one would expect a dominant absorption feature at $\Delta+U_{pd}$, modified by a typical hybridization energy. Clearly, this transition is observed for the undoped conductivity $\sigma'(\omega)$ (solid lines) in Figs. 12(a) and 12(b), where it is labeled A. For $\Delta=4$, $U_{pd}=0$ [Fig. 12(a)], this charge-transfer optical weight extends above $\omega\simeq4$, whereas for $\Delta=2$, $U_{pd}=1$ [Fig. 12(b)] it extends already above $\omega\simeq3$. As stressed before, in both cases, the minimum single-particle gap E_{CT} is found to be essentially the same. The physics behind this difference is clearly the excitonic effect.

Because of an attractive interaction ($-U_{pd}$) between the hole (now on O) and the "electron" left behind on Cu, it shifts in the two-particle excitations the optical energy downward by about U_{pd} compared to the single-particle excitations. Measurements of the optical conductivity[3,19] in $La_{2-x}Sr_xCuO_4$ (see, for example, Fig. 13) reveal strong absorption above 2 eV with a peak around 2.5–3 eV in the undoped system ($x=0$).

Thus, we have the interesting fact that, when we aim at simultaneously reproducing the single-particle (E_{CT}) and the two-particle charge-transfer gaps, we are led to a U_{pd} of the order 1. Of course, this is susceptible still to the finite-size effect, which also tends to shift the higher-energy transitions to somewhat lower energies. However, we should emphasize that we have found essentially no influence when increasing the system size from $N=12$ to $N=18$ sites.

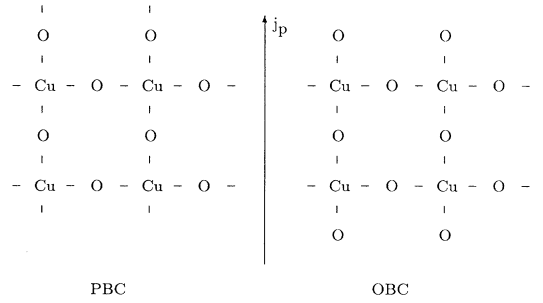

FIG. 11. Different geometries used for the two-particle correlation functions with open (OBC) and periodic (PBC) boundary conditions.

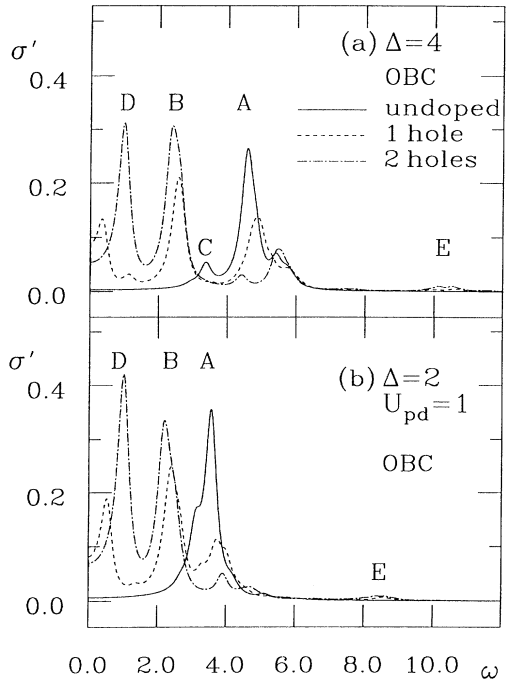

FIG. 12. σ' vs ω for the two parameter sets (a) and (b) (in both sets $U_d=6$, $U_p=3$) using OBC.

Comparison with the photoemission spectrum in Fig. 8 reveals that the charge-transfer peak A corresponds to transitions from nonbonding oxygen (NBO) to the upper Hubbard (UHB) band.

The onset of optical structure in the undoped situation is governed by a peak C in Fig. 12(a) [or the small shoulder on the low-energy side of peak A in Fig. 12(b)]. This peak is due to a transition of a Cu hole (UHB) to the correlated Zhang-Rice type of states denoted by (CS) in the single-particle spectra. Again this clearly is interesting in view of the common interpretation of the experimentally observed onset around 2 eV as being related to $d\rightarrow p$ charge transfer (A) only.[35]

Doping with holes results in a reduction of the spectral weight of A and a small shift to higher energies. This result, and also the shift of spectral weight to lower energies, as observed in Figs. 12(a) and 12(b) for one- and two-hole doping, are again found to be in general accord with experiments (see Fig. 13).

The lower-energy structure in the doped case (one hole: dashed lines; two holes: dash-dotted lines) in Fig. 12 consists of two peaks D and B. Comparison of the OBC spectrum with the PBC absorption in Fig. 14 (see the analog discussion for the 1D case in Sec. II C) clearly estab-

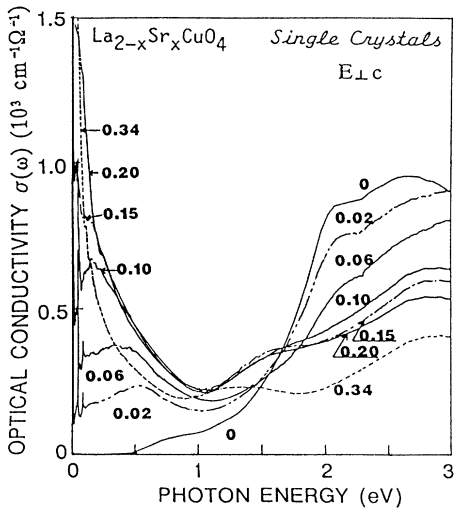

FIG. 13. Optical conductivity spectra of $La_{2-x}Sr_xCuO_2$ for various x (Tajima, Tanaka, Ido, and Uchida, Ref. 19).

lishes D as the Drude precursor to be expected for OBC at the finite energy ω_D: Thus, doping induces an insulator-metal transition. Again in accordance with our discussion in Sec. II C, the intensity of the Drude peak is strongly enhanced when going from the one-hole to the two-hole doped situation. The Drude weight has also been extracted using the expression (2.20) and found to be proportional to the number of doped carriers.

Two additional features B and E are observed in Fig. 12, both of which belong to transitions of holes out of the Zhang-Rice–type correlated states (CS). B is an excitation from CS to NBO and E from CS to LHB. The excitation energy in the photoemission spectrum, which belongs to E, is significantly different from the two-particle, i.e., optical excitation energy. It should be noted that in our 2×2 unit-cell system, the UHB–LHB excitation cannot be observed because of the selection rules embedded in the current operator.

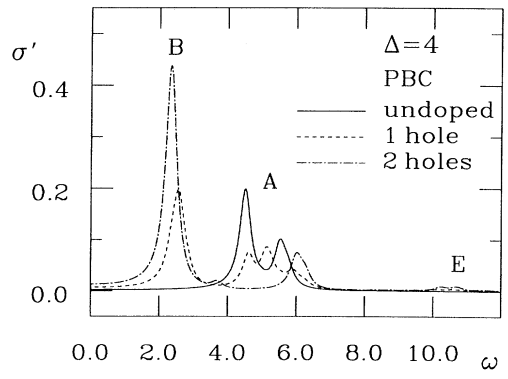

FIG. 14. σ' vs ω for $\Delta=4$, $U_d=6$, $U_p=3$, and periodic boundary conditions. As in the 1D situation, σ' contains no Drude part for the PBC case because σ' refers only to interband transitions.

Another interesting observation contained in Fig. 12 is that, while the charge-transfer peak A is substantially shifted by going from (a) to (b) parameter sets, the lower-energy structures D and B are not. This implies that the low-energy physics contained both in the single-particle and two-particle excitations is unaffected by the two different parameter choices, with U_{pd} just acting as an addition to the single-particle transition energy. As is to be expected, this no longer holds for the actual charge-transfer energy with its bare value $\Delta+2U_{pd}$ being reduced by the excitonic effect, which sets in only at this higher-energy scale.

In the one-hole doped spectrum we observe in Fig. 12(a) a small absorption structure between D and B. This structure is due to transitions within the correlated states (CS) in the single-particle spectra. It may be identified as the midinfrared peak discussed recently in connection with exact-diagonalization studies of the t-J model.[13,36,37]

Finally, if we apply periodic boundary conditions, the optical conductivity, as displayed in Fig. 14, no longer contains the Drude precursor at finite $\omega=\omega_D$. Its weight has been calculated from Eq. (2.9). Again, in the PBC case, one finds the structures B and A, which have already been identified as CS to NBO transitions and charge-transfer transitions in the OBC case with essentially unchanged excitation energies ω.

To analyze the Drude peak with help of the formulas given in Sec. II, we calculate the sum rule for both boundary conditions. Because of the small system size, and in accordance with Sec. II, we obtain with PBC a finite Drude weight D even for the undoped case $n=1$ ($x=0$). The very rough scaling possible with $N=18$ sites ($N_y=6$ in current direction) is in accordance with the exponential disappearance of D found for larger 1D systems in Sec. II C for the half-filled undoped case. For example, calculating the Drude weight from Eq. (2.9) with the parameter set (a) ($\Delta=4$, $U_d=6$, $U_p=3$) we obtain in the undoped system for $N=12$ sites $D=0.27$ and for $N=18$ sites $D=0.01$. However, doping the system results in a finite positive Drude weight indicating metallic behavior, which can be measured directly using OBC [Eq. (2.20)]. In this case the Drude weight increases roughly linearly with doping, in overall agreement with the experimental situation in Fig. 13: For $\Delta=4$ D is enhanced from 0.16 (one hole) to 0.39 for two holes [$\Delta=2$, $U_{pd}=1$: 0.25 (one hole)$\rightarrow$0.55 (two holes)].

C. Magnetic excitations of the three-band model

With exact diagonalization one can measure the spectral weight of the spin-spin correlation function,

$$\mathrm{Im}\chi(\mathbf{q},\omega)=\pi\sum_{n\neq0}\langle0|S^{z,\mathrm{Cu}}_{-\mathbf{q}}|n\rangle\langle n|S^{z,\mathrm{Cu}}_{\mathbf{q}}|0\rangle \times\delta(\omega-(E_n-E_0))\,, \tag{3.5}$$

where

$$S_{\mathbf{q}}^{z,\mathrm{Cu}}=\sum_i S_i^{z,\mathrm{Cu}} e^{i\mathbf{q}\cdot\mathbf{R}_i} \tag{3.6}$$

and $S_i^{z,\mathrm{Cu}}=\frac{1}{2}(n_{i\uparrow}^{\mathrm{Cu}}-n_{i\downarrow}^{\mathrm{Cu}})$. At $\mathbf{q}=(\pi,\pi)$ this correlation function can serve as a probe of the antiferromagnetic order at and near half-filling.

Our results for the half-filled and the one-hole doped cases are plotted in Fig. 15. In this calculation we concentrate on the same parameter sets [(a) $\Delta=4$, $U_{pd}=0$, and (b) $\Delta=2$, $U_{pd}=1$; in both sets we have chosen $U_d=6$ and $U_p=3$] used for the photoemission and the optical spectra. As shown in Sec. III A, both parameter sets guarantee insulating behavior because of a charge-transfer gap in the undoped half-filled case. In the undoped situation, we observe just one dominant feature at about 0.1 (in units of t_{pd}, as everywhere) for both parameter sets.

Consider for the sake of simplicity of argument just two neighboring Cu sites 1 and 2 antiferromagnetically coupled by the exchange constant J in strong coupling; i.e.,

$$H=J\mathbf{S}_1^{\mathrm{Cu}}\cdot\mathbf{S}_2^{\mathrm{Cu}} . \tag{3.7}$$

We note that the spin operator $S_{\mathbf{q}=(\pi,\pi)}^{z,\mathrm{Cu}}=S_1^z-S_2^z$ maps the singlet ground state $|0\rangle$ onto the triplet excited state $|1\rangle$, where

$$\left.\begin{matrix}|0\rangle\\|1\rangle\end{matrix}\right\}=\frac{1}{\sqrt{2}}(c_{1\uparrow}^{\dagger}c_{2\downarrow}^{\dagger}\mp c_{1\downarrow}^{\dagger}c_{2\uparrow}^{\dagger})|\mathrm{vac}\rangle . \tag{3.8}$$

Thus, we have $E_1-E_0=0.13$ for $\Delta=4$ (0.15 for $\Delta=2$, $U_{pd}=1$) in the diagonalization results. Due to the specific geometry of our 2×2 system this value must be compared with $2J_{\mathrm{Cu}}=0.17$ [0.20 for parameter set (b)], where J_{Cu} is given in strong coupling:[27,31–33]

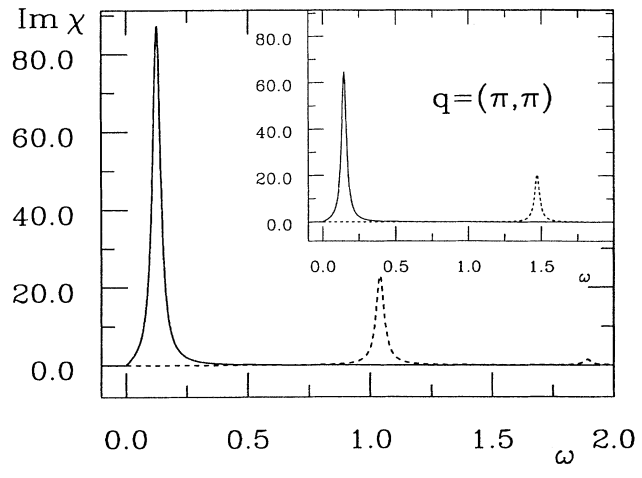

FIG. 15. Imaginary part of the magnetic susceptibility as a function of ω for $\Delta=4$, $U_d=6$, $U_p=3$, and (in the inset) $\Delta=2$, $U_{pd}=1$, $U_d=6$, and $U_p=3$. Solid lines denote the undoped case and dashed lines the one-hole doped situation.

$$J_{\mathrm{Cu}}=\frac{4t_{pd}^4}{(\Delta+U_{pd})^2}\left[\frac{1}{\Delta+U_p/2}+\frac{1}{U_d}\right] . \tag{3.9}$$

In the one-hole doped situation, the signal corresponding to Cu-Cu singlet-triplet excitations is not found. We interpret this fact as being caused by the delocalized nature of the Cu-O singlet, where the additional O hole polarizes the Cu spins not just at the two nearest-neighbor positions but all over our 2×2 unit cell system. Correspondingly, we expect the appearance of Cu-Cu singlet-triplet excitations for a larger-sized system for small dopings.

The additional structure in the doped situation at 1.04 for $\Delta=4$ (1.47 for $\Delta=2$, $U_{pd}=1$) can again be identified, following the same arguments as above, as stemming from a nearest-neighbor Cu-O Kondo-like spin coupling, replacing the site 2, say, by an O site in Eqs. (3.7) and (3.8). The strong-coupling value for the Cu-O singlet-triplet splitting,[27,31–33]

$$2J_{\mathrm{Kondo}}=2t_{pd}^2\left[\frac{1}{\Delta+U_p}+\frac{1}{U_d-\Delta-2U_{pd}}\right] , \tag{3.10}$$

is again found in good accord with the numerical value in Fig. 15 (1.04 versus $2J_{\mathrm{Kondo}}=1.29$ for $\Delta=4$; 1.47 versus $2J_{\mathrm{Kondo}}=1.4$ for $\Delta=2$, $U_{pd}=1$). Going to the thermodynamic limit will further shift down the numerical peak position.

Thus, the dynamical magnetic structure factor contains at higher energies and well separated from the lower-energy Cu-Cu transition Cu-O Kondo-like excitations. They are even further separated including a finite p-d Coulomb repulsion U_{pd}. This picture is also in general accordance with the basic physical assumption underlying the Zhang-Rice mapping, i.e., the formation of a tightly bound spin-singlet between a localized Cu spin and the dopant-induced hole carrier. This fact has recently been noted also for the Kondo-Heisenberg limit of the three-band Hubbard Hamiltonian.[38]

IV. SUMMARY

Two-particle optical and magnetic as well as single-particle excitations have been calculated via exact diagonalization for a one-dimensional (1D) Hubbard model and for a 2D multiorbital model appropriate for the cuprate superconductors. In 1D, particular emphasis has been placed on a numerical scaling analysis of the Drude weight D. Varying the system size N up to $N=12$ for different values of U/t and band fillings, it was found that D vanishes exponentially at half-filling with N on a length scale set by the inverse gap. However, for finite-sized rings with $N=4n$ D is negative ($4n+2$, positive) signaling paramagnetic response and an interesting violation of Lenz's law. Away from half-filling D tends to a diamagnetic positive value, thus being a direct probe of the Mott-Hubbard transition.

The 1D results on the low-frequency optical spectral weight and its finite-size dependence near the metal-insulator transition prepared the ground for a corresponding study in two dimensions. The single-particle excitations in the multiband 2D case display strongly

correlated states, related to the Zhang-Rice singlet construction. These states define the gap to the upper Hubbard band at half-filling and become partially occupied by doping one or two holes in our 2×2 unit-cell system. Various reasonable parameter sets with and without the p-d interaction U_{pd} yield this single-particle gap in agreement with experimental data. If, however, the optical excitations are also calculated with Lanczos diagonalization, the excitonic effect caused by U_{pd} was found to be essential for reconciling theoretical trends and experiment. To study the finite-size effect, system sizes up to $N=18$ have been diagonalized at half-filling.

Doping with one and two holes for 12-site lattices introduces a shift of absorption weight from the high-energy side to the low-energy side, in general agreement with experiment. Also in accord with experimental data is the observed reduction and shift to somewhat higher energies of the charge-transfer–related excitations. Three additional structures can clearly be identified on the low-energy side: First, the Drude peak and its weight ($\sim x$) have been extracted employing the techniques outlined already for the 1D case, both for PBC and OBC. Second, we found a small structure caused by internal transitions in the Zhang-Rice singlet structure which may be related to the experimentally observed midinfrared absorption. Additionally a strong absorption structure, which has not yet been reported in Hubbard-model studies, and which is caused by a transition from Zhang-Rice singlet states into the upper Hubbard band, was detected. We believe that this structure is very likely related to experimental optical weight found in the conductivity between the Drude and the charge-transfer peaks.

A general result that has emerged from our optical studies is that not only the low-energy physics as contained in t-J–type models, but also the higher-energy physics as measured in typical optical data between a fraction of an eV up to several eV's is significantly influenced by the Zhang-Rice–type Cu-O singlets: The Drude peak, as well as the small midinfrared absorption feature are caused by itinerant singlet motion. Furthermore, the new pronounced peak originating from the Zhang-Rice to nonbonding O-band transitions corresponds to the unbinding of the O hole from the Cu-O singlet.

We have finally also calculated the dynamic magnetic structure factor. The interesting feature here is that, for the doped situation, this structure factor displays a peak at the Kondo spin(O)-spin(Cu) correlation energy $2J_{\mathrm{Kondo}}\sim1-2$ eV. This signal, which has previously been detected in a simplified model,[38] stems from the Zhang-Rice type of singlet-triplet excitations and is expected to be observable in magnetic experiments.

ACKNOWLEDGMENTS

We would like to thank Professor W. Kohn, Professor R. J. Schrieffer, Dr. R. M. Fye, Dr. W. Stephan, Dr. P. Horsch, and Dr. D. Poilblanc for useful and stimulating discussions. Furthermore, we are grateful to Dr. E. Y. Loh for sending us a version of his Lanczos routine. We also thank Professor S. Uchida for the experimental data of the optical conductivity for $La_{2-x}Sr_xCuO_4$. One of us (W.H.) gratefully acknowledges the hospitality of the Department of Physics, University of California, Santa Barbara. J.W. and W.H. acknowledge support by the Bundesministerium für Forschung und Technologie (BMFT) Program No. 13 N 5501.

*Permanent address: Physikalisches Institut, Universität Würzburg, Am Hubland, D-8700 Würzburg, Germany.

[1]See, for example, P. A. Lee, T. M. Rice, J. W. Serene, L. J. Sham, and J. W. Wilkins, Comments Condens. Matter Phys. **12**, 99 (1986), and references therein.

[2]J. G. Bednorz and K. A. Müller, Z. Phys. B **64**, 189 (1986).

[3]*Proceedings of the International Conference on Materials and Mechanisms of Superconductivity–High-Temperature Superconductors II* [Physica C **162-164**, (1989)], and references therein.

[4]P. W. Anderson, Science **235**, 1196 (1987).

[5]V. J. Emery, Phys. Rev. Lett. **58**, 2794 (1987).

[6]P. F. Maldague, Phys. Rev. B **16**, 2437 (1977).

[7]D. Baeriswyl, C. Gros, and T. M. Rice, Phys. Rev. B **35**, 8391 (1987); D. Baeriswyl, J. Carmelo, and A. Luther, Phys. Rev. B **33**, 7247 (1986).

[8]E. Y. Loh, (unpublished); E. Y. Loh, T. Martin, P. Prelovšek, and D. K. Campbell, Phys. Rev. B **38**, 2494 (1988).

[9]B. S. Shastry and B. Sutherland, Phys. Rev. Lett. **65**, 243 (1990).

[10]H. J. Schulz, Phys. Rev. Lett. **64**, 2831 (1990).

[11]A. J. Millis and S. N. Coppersmith, Phys. Rev. B **42**, 10 807 (1990).

[12]X. Zotos, P. Prelovšek, and I. Sega, Phys. Rev. B **42**, 8445 (1990).

[13]W. Stephan and P. Horsch, Phys. Rev. B **42**, 8736 (1990).

[14]D. Poilblanc and E. Dagotto (unpublished).

[15]R. Fye, M. Martins, D. J. Scalapino, J. Wagner, and W. Hanke (unpublished).

[16]W. Kohn, Phys. Rev. **133**, A171 (1964).

[17]F. C. Zhang and T. M. Rice, Phys. Rev. B **37**, 3759 (1988).

[18]P. Horsch *et al.*, Physica C **162-164**, 783 (1989).

[19]For recent absorption experiments on $La_{2-x}Sr_xCuO_4$ crystals, see, for example, S. Tajima, S. Tanaka, T. Ido, and S. Uchida, in *Proceedings of the 2nd International Symposium on Superconductivity, Tsukuba, Japan,* edited by T. Ishiguro and K. Kajimura (Springer, Berlin, 1990); S. Uchida, H. Takagi, and Y. Tokura, Physica C **162-164**, 1677 (1989).

[20]See, for example, J. H. Wilkinson, *The Algebraic Eigenvalue Problem* (Clarendon, Oxford, 1965).

[21]R. Haydock, V. Heine, and M. J. Kelly, in *Solid State Physics,* edited by H. Ehrenreich, F. Seitz, and D. Turnbull (Academic, New York, 1980), Vol. 35.

[22]E. R. Gagliano and C. A. Balseiro, Phys. Rev. B **38**, 11 766 (1988).

[23]F. Mila, Phys. Rev. B **38**, 11 358 (1988).

[24]A. K. McMahan, R. M. Martin, and S. Satpathy, Phys. Rev. B **38**, 6650 (1988); A. K. McMahan, J. F. Annett, and R. M. Martin (unpublished).

[25]M. Schlüter, M. S. Hybertsen, and N. E. Christensen, Physica C **153-155**, 1217 (1988); Phys. Rev. B **39**, 9028 (1989).

[26]N. Nücker *et al.*, Phys. Rev. B **37**, 5158 (1988); J. Fink *et al.*,

in *Earlier and Recent Aspects of Superconductivity,* Vol. 90 of *Springer Series in Solid-State Sciences,* edited by J. G. Bednorz and K. A. Müller (Springer-Verlag, Berlin, 1990).
[27]J. Zaanen and A. M. Olés, Phys. Rev. B **37**, 9423 (1988).
[28]G. Dopf, A. Muramatsu, and W. Hanke, Phys. Rev. B **41**, 9264 (1990).
[29]R. T. Scalettar, D. J. Scalapino, R. L. Sugar, and S. R. White (unpublished).
[30]F. C. Zhang, Phys. Rev. B **39**, 7375 (1989).
[31]J. Wagner, A. Muramatsu, and W. Hanke, Phys. Rev. B **42**, 2200 (1990).
[32]V. J. Emery and G. Reiter, Phys. Rev. B **38**, 4547 (1988).
[33]A. Ramšak and P. Prelovšek, Phys. Rev. B **40**, 2239 (1989).
[34]P. Horsch (unpublished).
[35]S. Tajima *et al.,* J. Opt. Soc. Am. B **6**, 475 (1989).
[36]P. Prelovšek *et al.* (unpublished).
[37]A. Moreo and E. Dagotto, Phys. Rev. B **42**, 4786 (1990).
[38]C.-X. Chen, H.-B. Schüttler, and A. J. Fedro, Phys. Rev. B **41**, 2581 (1990).